Multi-Feature Driven Active Contour Segmentation Model for Infrared Image With Intensity Inhomogeneity

Qinyan Huang
Nanjing University of Science and Technology
Weiwen Zhou
Shanghai Institute of Spaceflight Control Technology
Minjie Wan
Nanjing University of Science and Technology School of Electronic and Optical Engineering
Xin Chen
Nanjing University of Science and Technology School of Electronic and Optical Engineering
Kan Ren
Nanjing University of Science and Technology School of Electronic and Optical Engineering
Qian Chen
Nanjing University of Science and Technology School of Electronic and Optical Engineering
Guohua Gu (gghnjust@mail.njust.edu.cn)
Nanjing University of Science and Technology School of Electronic and Optical Engineering

Research Article

Keywords: infrared image segmentation, active contour model, signed pressure force function, local feature, adaptive weight coefficient

Posted Date: March 15th, 2021

DOI: https://doi.org/10.21203/rs.3.rs-292034/v1

Noname manuscript No.
(will be inserted by the editor)

Multi-feature driven active contour segmentation model for infrared image with intensity inhomogeneity

Qinyan Huang [1] · Weiwen Zhou [2] · ✉Minjie Wan [1] · Xin Chen [1] · Kan Ren [1] · Qian Chen [1] · ✉Guohua Gu [1]

the date of receipt and acceptance should be inserted later

Abstract Active contour model (ACM) is one of the most widely used image segmentation tools at present, but the existing methods only utilize single feature information of image to minimize the energy function, which is easy to cause false segmentations in infrared (IR) images. In this paper, we propose a multi-feature driven active contour segmentation model to handle IR images with intensity inhomogeneity. Firstly, an especially-designed signed pressure force (SPF) function is constructed by combining the global information calculated by global average gray information and the local multi-feature information calculated by local entropy, local standard deviation and gradient information. Then, we draw upon adaptive weight coefficient computed by local range to incorporate the afore-mentioned global term and local term. Next, the SPF function is substituted into the level set formulation (LSF) for further evolution. Finally, the LSF converges after a finite number of iterations and the IR image segmentation result is obtained from the corresponding convergence result. Experimental results demonstrate that the presented method outperforms typical models in terms of precision rate and overlapping rate in IR test images.

Keywords infrared image segmentation · active contour model · signed pressure force function · local feature · adaptive weight coefficient

1 Introduction

With the development of IR imaging and computer vision [1], image segmentation which aims to extract object of interest from image plays an essential

Minjie Wan E-mail: minjiewan1992@njust.edu.cn
Guohua Gu E-mail: gghjust@mail.njust.edu.cn
1 School of Electronic and Optical Engineering, Nanjing University of Science and Technology, Nanjing 210094, China
2 Shanghai Institute of Spaceflight Control Technology, Shanghai 201109, China

role in many areas of both civil and military applications, such as geology exploration [2], aerospace engineering [3], security monitoring [4] and so on. Among various image segmentation methods [5–8], ACM has gained popularity because of its excellent ability to obtain closed contours with sub-pixel accuracy [9]. Although, a number of ACMs [10–13] have achieved satisfactory performances in clear visible images, they only use single image feature information to construct the energy function. Therefore, the results may suffer from false segmentations when the traditional ACMs are directly applied to handle IR images with intensity inhomogeneity, blurred boundary and low contrast. From the above, it is of great necessity to especially design an effective ACM for IR target segmentation.

Conventional ACMs usually utilize edge information or statistical intensity information to design the energy functional [14]. The edged-based models stop the contour evolution by an edge stopping function (ESF) which is calculated by the gradient information of image. Usually, an ESF has the property that the larger gradient is, the smaller value of ESF is. Geodesic active contour (GAC) model [15] is a representative edge-based model, but this model can achieve desirable segmentation results when the initial contour is set on specific location surrounding the real boundary. In addition, it is quite sensitive to the interference of noise because the construction of ESF is completely based on gradient information. Paragions et al. [16] improved GAC model by using the gradient vector field and a balloon force so that it can converge accurately near the target boundary. Meanwhile, additive operator splitting (AOS) is introduced to speed up the computing of the model. Wang et al. [17] redefined the energy functional by imposing regional information to improve the boundary leaking problem of the original GAC model. Using the global average intensity information inside and outside the evolving curve [18], a lot of region-based ACMs have been proposed. Chan-Vese (CV) model [19] represents intensity of object and background by average intensity constants inside and outside contour. In this way, it can segment images with intensity homogeneity effectively, but false segmentation will occur when the intensity distribution of object is inhomogeneous. To make up for the deciencies of CV model, local intensity information is imposed to construct the LSF. The local binary fitting (LBF) model, proposed by Li et al. [20], uses Gaussian kernel function to construct the local energy function. Related experiments show that LBF model outperforms CV model in handling inhomogeneous IR images, however it is prone to local minimum and is sensitive to initialization. For faster and more accurate image segmentation, Ding et al. [21] proposed local pre-fitting (LPF) model in which local average image intensities are used to form two pre-fitting functions. Because pre-fitting functions are calculated before the curve evolution, they are invariant during the iterations. By this means, the computational time of LPF model decreases remarkably. Local region-based Chan-Vese (LRCV) model developed [22] by Liu et al. constructs the energy functional using local average intensity information in order to extract objects with intensity inhomogeneity correctly. Wang et al. [23] designed entropy weighted fitting (EWF) model, in which Kullback Leibler divergence

is introduced as a measuring metric for comparing the input image and three local fitting images and inhomogeneity entropy descriptor is regard as weight to adjust the afore-discussed images. Laplacian of Gaussian (LoG) which is an essential second-order dierential operator can detect the edge of image effectively while region-scalable fitting (RSF) which imposes kernel function to estimate local intensity is a local region-based model. By combining the advantages of these two terms, Ding et al. [24] put forward LoG & RSF model to alleviate the sensitivity to contour initialization of RSF model and achieves more accurate segmentation results in related experiments. However, the LoG operator is sensitive to the change of intensity, when the boundaries of images are blurred and background regions are complex, some false edges will still occur. Another strategy to cope with inhomogeneity is to combine ACMs with bias field estimation. Li et al. [25] proposed local intensity clustering (LIC) model via replacing the average intensity constant with a local cluster function and the inhomogeneous regions can be corrected by the estimated bias field. However, the clustering variance is not taken into consideration and the process of minimizing the energy functional is time-consuming. Locally statistical active contour model (LSACM) [26] can be categorized into K-means clustering method. It defines a clustering criterion to combine pixels of the same class effectively and is able to obtain a complete segmentation contour. Huang et al. [27] designed a region-based SPF function in order to handle inhomogeneous images correctly. Furthermore, the kernel function used for regularizing LSF is constrained by an adaptive scale parameter and the bias field is initialed in a new way, so this model can estimate the bias field more accurately and the contour can be initialized in arbitrary locations. Hai et al. [28] put forward a region-bias fitting (RBF) model to deal with inhomogeneous images by proposing a constraint term with region bias. Using local difference between the input image and the bias estimated image, Shan et al. [29] developed local region-based fitting (LRBF) model in which neighborhood of every pixel constructs a local energy function and these functions are then integrated to form a total energy functional. In addition, there are some other special ACMs. Zhang et al. [30] designed a novel model named the selective local or global segmentation (SLGS) model, which utilizes statistical information to form a SPF function and then substitutes the ESF of GAV model by the new SPF function. Mukherjee et al. [31] presented an edge independent segmentation model which estimates the object and background intensity by a series of Legendre polynomial functions and it is robust to the change of grayness. However, IR images have more complex properties e.g. intensity inhomogeneity, blurred boundary, and low contrast and so on [32]. Above-mentioned ACMs still cannot deal with IR target perfectly, so it is essential to design a special ACM for IR image segmentation.

In this paper, we propose a new ACM model by constructing SPF functions with both global and local information. The global term is to control the evolving curve to pass through the flat background region quickly and to prevent the evolving curve falling into local minimum. Based on this consideration, we choose global average intensity information to form the global term.

The local term consists of multi-features, including entropy, standard deviation and gradient, which accurately guides the convergence of the evolving curve when it is close to the real edge. At the same time, we calculate the adaptive weight coefficient based on local range information in order to incorporate the global term and local term. Then, the afore-mentioned SPF function is used to construct the LSF, and Gaussian filter is also utilized to regularize the LSF for the purpose of removing the re-initialization process. By a finite number of iterations, LSF tends to converge, and its zero LSF is taken as the contour boundary of object.

The main contributions of this paper can be summarized as follows:

(1) Average intensity information inside and outside the contour is combined to form the global term, which prevents the curve evolution falling into local minimum.

(2) Local multi-feature information is introduced to construct a new SPF function for overcoming the interference of intensity inhomogeneity.

(3) An adaptive weight coefficient calculated by local range information is proposed to guide the evolution of active more effectively.

The rest of this work is organized as below. First, the motivation of our study is discussed in Section 2. Section 3 introduces the theory of our proposed ACM in detail, especially the construction method of the new SPF function. Comparative experimental are presented in Section 4 and a brief summary is drawn in Section 5.

2 Motivation

Zhang et al. [30] developed an SLGS model on the assumption that image intensities are statistically homogeneous. As shown in Eq. (1), the LSF ϕ is initialized to a constant and the sign of constant is opposite inside and outside the contour.

$$\phi\left((u,v),t=0\right)=\begin{cases}-c_0,(u,v)\in\Omega_0-\partial\Omega_0\\0,(u,v)\in\partial\Omega_0\\c_0,(u,v)\in\Omega-\Omega_0\end{cases}\tag{1}$$

where constant $c_0>0$, Ω denotes the input image and Ω_0 represents a subset of the Ω; The zero level of ϕ corresponds to the boundary of Ω_0 and it is described as $\partial\Omega_0$. Then, the model uses the average intensity information to form a SPF function and its values are normalized in the range [-1, 1]. Note that the role of SPF function is to determine the evolution direction. More specifically, the curve shrinks when it is outside of the object and expands when it is inside of the object. For a given IR image $I\left(u,v\right)$, the SPF function is defined as:

$$spf\left(I(u,v)\right)=\frac{I(u,v)-\frac{c_1+c_2}{2}}{\max\left|I(u,v)-\frac{c_1+c_2}{2}\right|}\tag{2}$$

where c_1 and c_2 serve as the average intensities inside and outside the contour, respectively. Their mathematical expression as follows:

$$c_1(\phi) = \frac{\int_\Omega I(u,v) \cdot H(\phi)\, dudv}{\int_\Omega H(\phi)\, dudv} \tag{3}$$

$$c_2(\phi) = \frac{\int_\Omega I(u,v) \cdot (1 - H(\phi))\, dudv}{\int_\Omega (1 - H(\phi))\, dudv} \tag{4}$$

where $H(\phi)$ means the regularized Heaviside function and it is defined as follows:

$$H_\varepsilon(\phi) = \frac{1}{2}\left(1 + \frac{2}{\pi}\arctan\left(\frac{\phi}{\varepsilon}\right)\right) \tag{5}$$

where ε is control factor; $H(\phi) = 1$ when $\phi > 0$,otherwise $H(\phi) = 0$. The LSF of SLGS model can be written as:

$$\frac{\partial \phi}{\partial t} = spf(I(u,v)) \cdot \alpha \cdot |\nabla \phi| \tag{6}$$

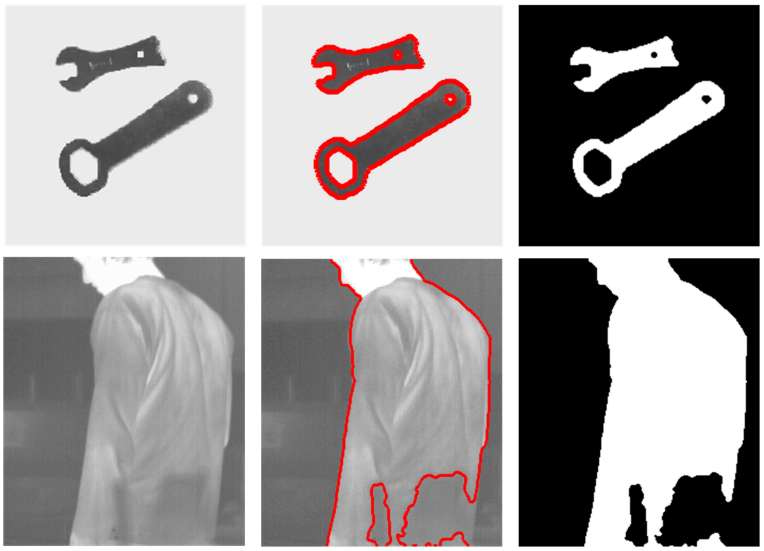

(a) (b) (c)

Fig. 1 Segmentation results of SLGS model: (a) original image; (b) segmentation result; (c) binary segmentation result.

As shown in the first row of Fig.1, SLGS model can obtain desirable segmentation result when the image intensities are statistically homogeneous in visible image. However, when it is applied to IR image with intensity inhomogeneity (see the second row of Fig.1), the segmentation precision significantly

decreases. This is because SLGS model assumes the grayness of both object and background is homogeneous and only uses average intensity constants to describe the intensity distribution. However, the object in IR image always contains intensity inhomogeneity, so this model no longer works in practice.

To overcome the afore-discussed deficiency of SLGS model, local feature information is introduced to guide the curve evolution in inhomogeneous regions. A special term which contains both global intensity information and local feature information is designed to replace the original SPF function. In this way, the new ACM can extract IR objects with intensity inhomogeneity effectively.

3 Theory

According to the analysis in Section 2, we know that SPF function which only contains global grayness information cannot segment IR image effectively. The key technique of this paper is to design a new SPF function by combining global gray information with local multi-feature information. Multi-feature information is introduced to highlight the difference in those regions with intensity inhomogeneity so that the evolution direction of curve can be determined more accurately. By the guidance of the new SPF, the presented ACM is able to segment inhomogeneous IR images correctly. The structure diagram of this work is shown in Fig.2.

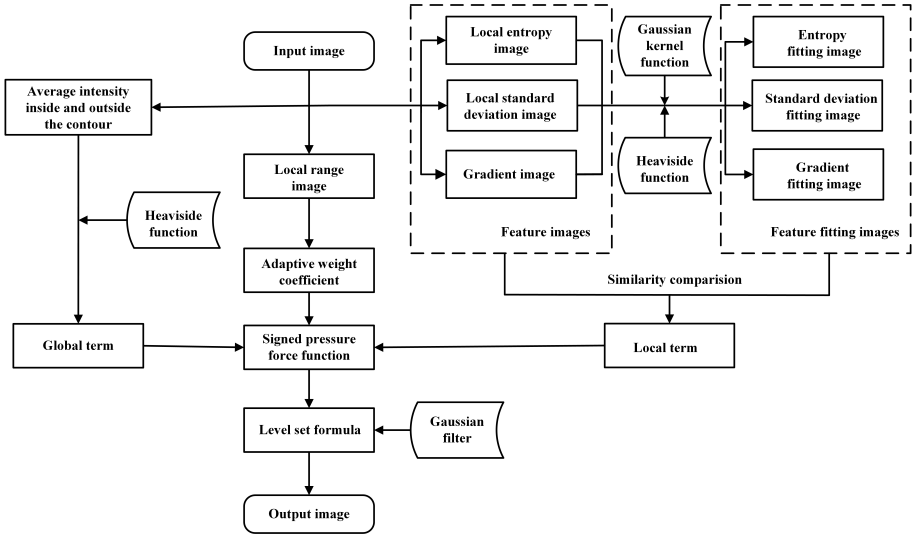

Fig. 2 Structure diagram of the proposed method.

3.1 Design of global term

The global term aims to prevent the curve falling into local minimum and drive the curve to pass through the flat background region quickly. Hence, for a given IR image I, we utilize global gray average information to form the global term and its calculation formula is described as:

$$SPF_{global}(u,v) = I(u,v) - (c_1 \cdot H(\phi) + c_2 \cdot (1 - H(\phi))) \tag{7}$$

where c_1 and c_2 are calculated by Eq. (3) and (4), respectively. The second term of Eq. (7) represents the fitting image and it can be constructed by combining the average intensities inside with outside the contour through Heaviside function $H(\phi)$. When the difference between the original image and the fitting image is the smallest, the SPF_{global} function tends to 0 and the curve stops evolving. Furthermore, the sign of SPF_{global} function can determine the direction of pressure forces, so that the evolving curve can shrink or expand to extract the object.

3.2 Design of local term

As far as we are concerned, it is inadequate to represent IR image with intensity inhomogeneity when only global gray information is considered. To determine a more precise evolution direction, local entropy, local standard deviation and gradient information are employed to construct the local term. We set a local window W_n whose size is $n \times n$ surrounding the center pixel (u, v),then the entropy image I_en, standard deviation image I_std and gradient image I_grad are computed by the following formulas:

$$I\_en(u,v) = \sum_{i=0}^{L} p_i \log p_i \left(p_i = \frac{n_i}{n \times n} \right) \tag{8}$$

$$I\_std(u,v) = \sqrt{\frac{1}{n \times n} \sum_{(u,v) \in W_n} (I(u,v) - \mu)^2} \tag{9}$$

$$I\_grad(u,v) = \sqrt{(I(u+1,v) - I(u,v))^2 + (I(u,v+1) - I(u,v))^2} \tag{10}$$

where L refers to the total number of gray levels in the local window; i means a certain gray value and n_i is the number of pixels corresponding to i; p_i is the probability of pixels with gray value i in the window; μ means the average gray level of all pixels in W_n and its calculation formula is $\mu = \frac{1}{n \times n} \sum_{(u,v) \in W_n} I(u,v)$.

To demonstrate the difference of feature information between object and background, as shown in Fig.3(a), three local areas of an example IR image (marked in red rectangle) are selected to make a deep analysis. As we can see from Fig.3(b), the selected local features have more remarkable difference inside and outside the contour when compared with global intensity, i.e., local

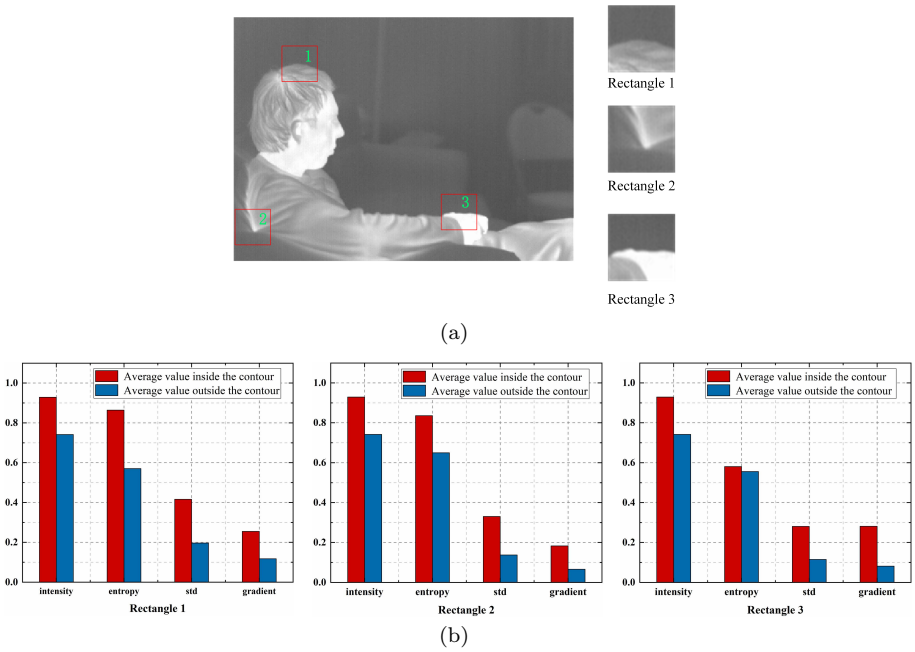

Fig. 3 Comparative analysis of local features: (a) local area of original image; (b) average values of different features in rectangle 1, rectangle 2 and rectangle 3 respectively, red charts represent the average of object, blue charts represent the average of background.

multi-features are able to provide more local information to guide the curve evolution. Therefore, we design a local term dominated by three local features to cooperate with the global term. In this way, the segmentation results in inhomogeneous regions can be more accurate.

According to LBF model [20], a Gaussian kernel function K_σ is introduced to embed the local intensity information, and the approximate local intensity calculation formulas inside and outside the contour are shown in Eq. (11) and (12).

$$f_{in}\left(u,v\right)=\frac{K_\sigma * \left[M_1\left(\phi\right)I(u,v)\right]}{K_\sigma * M_1\left(\phi\right)} \tag{11}$$

$$f_{out}\left(u,v\right)=\frac{K_\sigma * \left[M_2\left(\phi\right)I(u,v)\right]}{K_\sigma * M_2\left(\phi\right)} \tag{12}$$

where σ is standard deviation and $*$ represents the convolution operator; $M_1\left(\phi\right)=H\left(\phi\right)$, $M_2\left(\phi\right)=1-H\left(\phi\right)$ and $H\left(\phi\right)$ is given by Eq. (5). $f_{in}\left(u,v\right)$ and $f_{out}\left(u,v\right)$ denote the approximate image intensities in the neighborhood of pixel (u,v) inside and outside the evolving curve respectively. On this basis, we also impose a Gaussian kernel function K_σ to embed the local entropy, local standard deviation and gradient information. Their mathematical expressions

are as follows:

$$\Sigma_{in}(u,v)=\begin{cases} entro_{in}(u,v)=\frac{K_\sigma*[M_1(\phi)I\_en(u,v)]}{K_\sigma*M_1(\phi)} \\ std_{in}(u,v)=\frac{K_\sigma*[M_1(\phi)I\_std(u,v)]}{K_\sigma*M_1(\phi)} \\ grad_{in}(u,v)=\frac{K_\sigma*[M_1(\phi)I\_grad(u,v)]}{K_\sigma*M_1(\phi)} \end{cases} \tag{13}$$

$$\Sigma_{out}(u,v)=\begin{cases} entro_{out}(u,v)=\frac{K_\sigma*[M_2(\phi)I\_en(u,v)]}{K_\sigma*M_2(\phi)} \\ std_{out}(u,v)=\frac{K_\sigma*[M_2(\phi)I\_std(u,v)]}{K_\sigma*M_2(\phi)} \\ grad_{out}(u,v)=\frac{K_\sigma*[M_2(\phi)I\_grad(u,v)]}{K_\sigma*M_2(\phi)} \end{cases} \tag{14}$$

where $\Sigma_{in}(u,v)$ contains three types of local feature information inside the contour while $\Sigma_{out}(u,v)$ contains three types of local feature information outside the contour. Every feature information from both sides of the contour can be combined by Heaviside function to construct the single feature fitting image. The similarities are measured by calculating the distance between feature fitting images and original feature images. Thus, we can obtain three SPFs dominated by three local features respectively, which are defined as Eqs. (15-17):

$$spf\_en(u,v)=I\_en(u,v)-[entro_{in}(u,v)\cdot M_1(\phi)+entro_{out}(u,v)\cdot M_2(\phi)] \tag{15}$$

$$spf\_std(u,v)=I\_std(u,v)-[std_{in}(u,v)\cdot M_1(\phi)+std_{out}(u,v)\cdot M_2(\phi)] \tag{16}$$

$$spf\_grad(u,v)=I\_grad(u,v)-[grad_{in}(u,v)\cdot M_1(\phi)+grad_{out}(u,v)\cdot M_2(\phi)] \tag{17}$$

where spf_en, spf_std and spf_grad represent the driving forces provided by entropy, standard deviation and gradient information respectively. Then, the local term is computed as the sum of the three functions:

$$SPF_{local}(u,v)=spf\_en(u,v)+spf\_std(u,v)+spf\_grad(u,v) \tag{18}$$

By calculating Eq. (18), the local feature information is employed to provide pressure force and the evolution direction of every pixel on the curve can be thus determined.

3.3 Adaptive weight coefficient

In order to combine the afore-mentioned global and local term in our model more reasonably, the adaptive weight coefficient $\omega(u,v)$ is proposed to construct a complete SPF as follows:

$$SPF_{total}=\omega(u,v)\cdot SPF_{global}+(1-\omega(u,v))\cdot SPF_{local} \tag{19}$$

where SPF_{total} should be normalized to the range [-1,1]. As shown in Eq. (19), the value of $\omega(u,v)$ decides whether the SPF function is mainly driven by global term or local term. On the one hand, when the intensity of image region

changes remarkably, the global average gray information cannot represent the local intensity change and may result in false segmentation. At this point, local feature information is essential to be taken into consideration, i.e., the weight of local term SPF_{local} should be increased. On the other hand, when the intensity varies smoothly, it indicates that the contour is in the background region, so we should increase the weight of global term SPF_{global} in order to pass through the background region quickly. Hence, we choose local range to quantificationally reflect intensity variation, the mathematical formula of which can be written as:

$$range\left(u,v\right)=\max\left(W_m\left(u,v\right)\right)-\min\left(W_m\left(u,v\right)\right) \tag{20}$$

The significance of Eq. (20) is to compute the difference between maximum and minimum in the $m\times m$ sized local window W_m. According to the above-mentioned analysis, the weight coefficient $\omega\left(u,v\right)$ is designed as follows:

$$\omega\left(u,v\right)=\frac{1}{1+\lambda\cdot range\left(u,v\right)} \tag{21}$$

where $\omega\in(0,1)$ and λ is a constant. If the evolving curve is in the flat region without any objects, the value of local range is small, i.e., ω tends to 1, so the global term dominates the curve evolution. While the evolving curve is near the real boundary, the value of local range becomes large and ω tends to 0. At this time, curve evolution is mainly controlled by the local term. By this means, the weight of global term and local term can be adaptively determined by the new SPF function, leading to the advantage that our ACM can segment IR image with intensity inhomogeneity more effectively.

3.4 Implementation

By exploiting the new SPF function, the LSF can be rewritten as follows:

$$\frac{\partial\phi}{\partial t}=SPF_{total}\cdot\alpha\cdot|\nabla\phi|=\left[w\cdot SPF_{global}+(1-w)\cdot SPF_{local}\right]\cdot\alpha\cdot|\nabla\phi| \tag{22}$$

In traditional ACMs, Signed Distance Function (SDF) is used for the initialization of LSF and it depicts the shortest distance from a pixel to the evolving curve. Thus, when the location of evolving curve changes, the values of SDF also need to be updated, i.e., the process of re-initialization is necessary during the iterations. In order to reduce the computational time of SDF and re-initialization, in our model, the LSF ϕ is initialized to constant as Eq. (1) and a selective step is utilized to penalize LSF to be binary. Whether the selective step is performed depends on the desired property. If we only want to extract the object of interest, it is necessary; otherwise, it is unnecessary. Then Gaussian function is utilized to regularize the LSF after each iteration as:

$$\phi_t=\phi_{t-1}*G_{\sigma\_\phi} \tag{23}$$

where G_{σ_ϕ} represents a Gaussian function. ϕ_{t-1} means the evolution result of (t-1)-th iteration and ϕ_t can be considered as the initial state of t-th iteration. By executing Eq. (23), the procedure of re-initialization can be removed.

In order to stop evolution in time, we set a stopping criterion of curve evolution as follow:

$$|\phi_t - \phi_{t-1}| < \delta \tag{24}$$

where δ is convergence threshold and the Eq. (24) means the LSF does not change obviously any further.

To describe the implementation of our model clearly, the main procedures of the proposed algorithm are summarized as below:

Algorithm 1

Input: an IR image I .
initialize the LSF ϕ to be a binary function according to Eq. (1).
while not convergence **do**
  for every pixel **do**
    Construct the global term SPF_{global} according to Eq. (7);
    Construct the local term SPF_{local} according to Eq. (18);
    Compute the adaptive weight coefficient ω using Eq. (21).
  end for
  Construct complete SPF function using Eq. (19).
  Update the LSF according to Eq. (22).
  Regularize the LSF according to Eq. (23).
  if $|\phi_t - \phi_{t-1}| < \delta$ **then**
    break;
  end if
end while
Output: the zero-level set of $\phi : \phi((x, y), t) = 0$

4 Experimental results

Both qualitative and quantitative experiments are conducted with real IR images to demonstrate the accuracy and efficiency of our method in this section. All the experiments are implemented using Matlab 2016a on a PC with Intel Core i7-8565U, CPU 1.80GHz and RAM 8.0 GB.

4.1 Parameter Setting

According to the previous works and relevant experimental results, all related parameters mentioned in the study as well as their meanings and default values in our experiments are listed in Table.1.

Referring to LBF model [20], the standard deviation of Gaussian function K_σ utilized for embedding local feature information is σ= 3.0. The size of local window used for computing local features is fixed to be 9×9. LSF is initialized

Table 1 Initialization of Parameters

Parameter	Meaning	Setting Value
c_0	The constant used for initializing the LSF	1.0
σ	The standard deviation of the Gaussian kernel function used for embedding local features	3.0
n	The width of local window to calculate the feature information	9
m	The width of local window to calculate the adaptive coefcient	5
λ	Determine the weight of global term and local term	0.5
α	The balloon force of LSF	400
σ_ϕ	The standard deviation of the Gaussian filter used for regularizing LSF	1.0
δ	The convergence threshold	10^{-5}

to constant ρ and we set ρ= 1 as SLGS model. We use Gaussian filter whose standard deviation is σ_ϕ to re-initialize LSF. If σ_ϕ is set too small, the interference of noise may influence the segmentation result. While σ_ϕ is too large, it may cause inaccurate boundary detections. σ_ϕ ranges from 0.8 to 1.5 by experience and it set to be 1.0 in our experiments. We apply convergence threshold. δ= 10^{-5} as a criterion to stop the curve evolution in all comparative methods. λ determines the weight of global term and local term in Eq. (21) while α determines the convergence rate of the LSF in Eq. (22), and these two parameters influence the precision rate of segmentation significantly. Further sensitivity analysis about λ and α are presented below.

To obtain suitable settings of λ and α, we introduce F value to make sensitivity analysis in a quantitative way and it is defined as follows:

$$F = \frac{2 \cdot \mathrm{Pre} \cdot \mathrm{Rec}}{\mathrm{Pre} + \mathrm{Rec}} \tag{25}$$

where $F \in [0, 1]$; Pre represents the precision rate and Rec represents recall rate, whose computational formulas are given as:

$$\mathrm{Pre} = \frac{I_{cor}}{I_{out}} \tag{26}$$

$$\mathrm{Rec} = \frac{I_{cor}}{I_{truth}} \tag{27}$$

where I_{out} denotes the output binary image segmented by the ACMs; I_{truth} represents the binary image of ground truth; I_{cor} can be computed by following formula: $I_{cor} = I_{truth} \cap I_{out}$ and it refers to the correctly segmented region. Generally speaking, the larger F values is, the more accurate segmentation result is.

We select three types of IR images to make the sensitivity analysis about λ and α, All these images contain a degree of local intensity inhomogeneity, but they represent images with single object, images with multiple objects and images with low resolution, respectively. While other parameters are fixed, we set λ changing from 0 to 3 (the step length is set as 0.5) and the F value is calculated for each λ. The experimental result is drawn in Fig.4(a). These $F - \lambda$ curves indicate that along with the increase of λ, the F values tend to decrease. Focusing on the average curve (marked in red), we consider that the F values are acceptable when λ varies in the range [0,1]. It reaches the maximum when $\lambda = 0.5$, so we set $\lambda = 0.5$ in our experiments. As for α, it

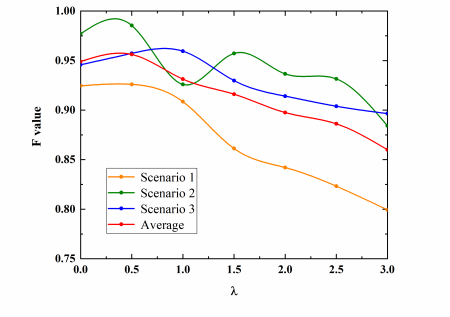

(a)

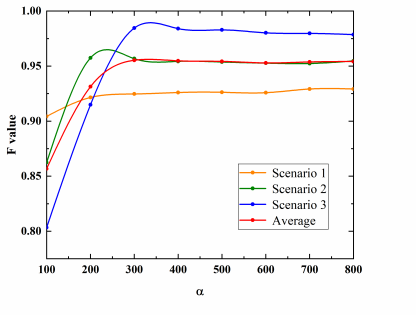

(b)

Fig. 4 Sensitivity analysis: (a)$F-\lambda$ curves; (b) $F-\alpha$ curves.

changes from 100 to 800 and the step length is chosen as 100. The $F-\alpha$ curves drawn according to experimental result are shown in Fig.4(b). We can see that the F values increase remarkably when α varies from 100 to 400, but the $F-\alpha$ curves are almost a straight line with high F values when $\alpha > 400$. Considering the segmentation efficiency, we finally adopt $\alpha = 400$ in our experiments. We would like to point out that the setting values listed in Table.1 are just reference values and they still need to be slightly adjusted when dealing with different IR images.

4.2 Comparative experiment

In order to compare our proposed method with other ACMs in qualitative and quantitative ways, 16 IR images which all contain a degree of inhomogeneity are selected to make comparative experiments. In particular,IR.7-IR.9 have similar characteristics with low contrast and blurred boundary. IR.1-IR.11 only contain a single object while the rest images have more than one object of interest. We compare the result of our method with 6 well-known ACMs:

GAC [15], CV [19], SLGS [30], LPF [21], LoG & RSF [24] and LIC [25] model which all have been discussed in Section 2.

4.2.1 Comparison of segmentation result

As shown in Fig.5, the original images are presented in the first column and we set uniform initial contour whose size is 40×40 in the image center for the ACMs (marked in green). Corresponding to columns (2-9), the segmentation results of GAC, CV, SLGS, LPF, LoG & RSF, LIC and proposed method, as well as the ground truth are shown respectively, in which the finally evolving curves are marked in red.

We notice that GAC model does not converge on all the test images due to its sensitiveness to the initialization of contour. According to Zhangs research [30], the object is able to be segmented correctly, only when the initial contour is set in the appropriate location. But in our experiments, contours are initialized in the image center, which does not satisfy this condition, the segmentation results of GAC model are thus unsatisfactory. CV model assumes that intensities of object and background are statistically homogeneous and it only utilizes global average intensity which is regarded as constant to construct the energy functional. However, IR image always involves a certain degree of inhomogeneity in practice. Hence, CV model always causes false segmentation in clothes region with intensity inhomogeneity. SLGS model combines the advantages of GAC and CV, thus it can handle IR images with blurred boundary and low contrast effectively (see IR7-IR.9 and IR16). Nevertheless, when the local intensity inhomogeneity of object is serious, SLGS model has the same drawback as CV model, i.e., false segmentation and boundary leakage occur in those inhomogeneous areas.

LPF model and LoG & RSF model are representative models of local tting-based ACMs. Energy functions of local fitting-based ACMs usually involve the local intensity information but ignore the global information, so they are sensitive to the state of initialization and always fall into local minima due to lack of global information. According to the segmentation results of LPF model and LoG & RSF model, we can verify the above-mentioned conclusion that they both fall into local minima, so the curve always stops evolving in the interior of object with remarkable segmentations errors. In particular, when the contrast of images is low (such as IR7, IR8 in Fig.4), the active contours of LPF model and LoG & RSF model almost stop evolving during the whole iterative procedure.

LIC model estimates the intensity in a neighborhood of each pixel by designing a local clustering criterion function and then integrates the local function to construct the total energy functional. Meanwhile, the bias field estimation is introduced to intensity inhomogeneity correction. Since the clustering variance is not taken into consideration, as we can see from the segmentation result, this model still cannot handle IR image region with serious intensity inhomogeneity effectively. In addition, this model is sensitive to the change of

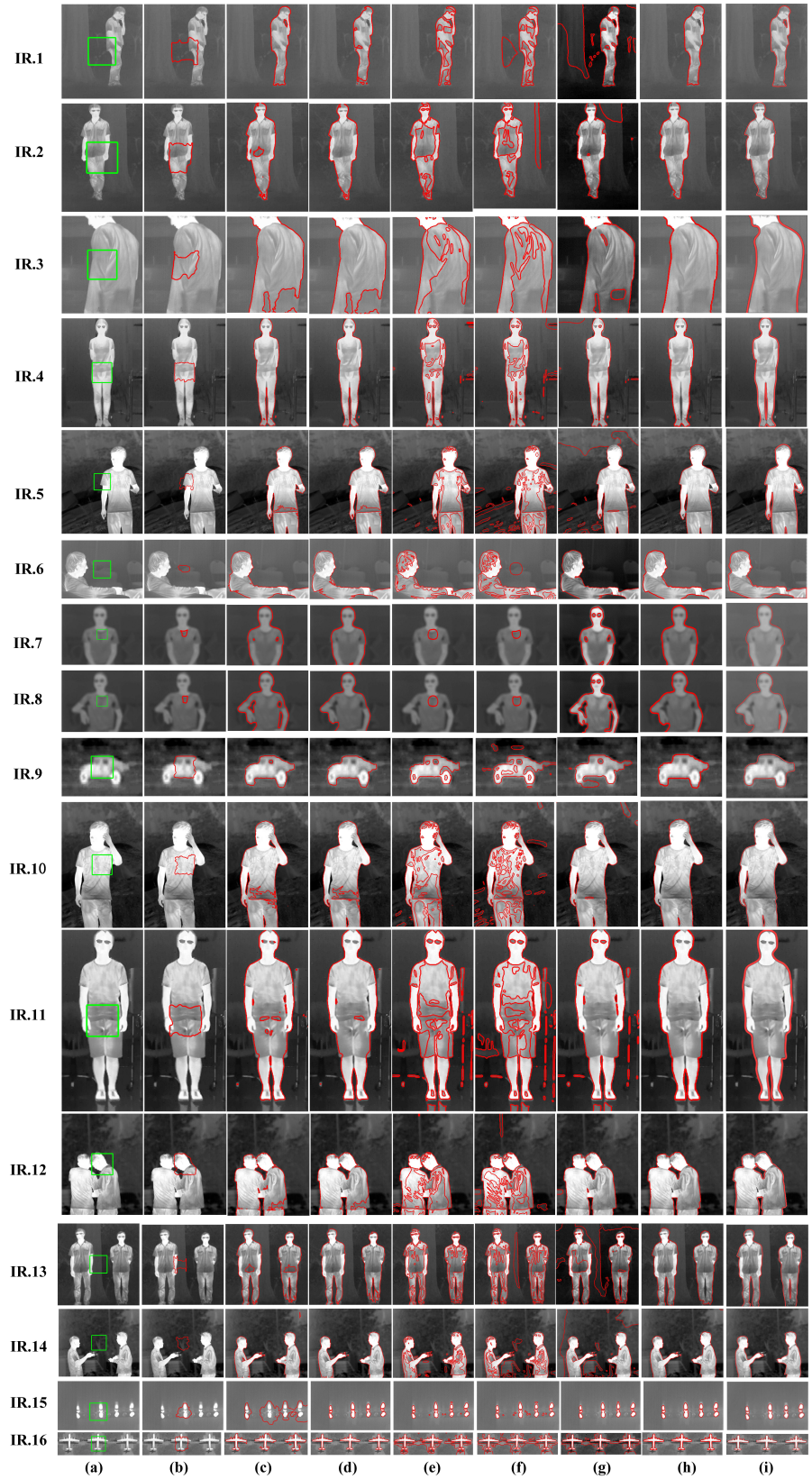

Fig. 5 Segmentation results of ACMs: (a) initial contour; (b) GAC; (c) CV; (d) SLGS; (e) LPF; (f) LoG & RSF; (g) LIC; (h) the proposed method; (i) ground truth.

intensity, so we can find that the contours do not converge in those background regions with intensity change (see IR1, IR2, IR5, IR13, IR14).

Compared with the conventional ACMs, this presented ACM performs more precisely and robustly in segmenting the test images, and it is worth noting that our method can effectively handle IR.4 and IR.11 which are contaminated by noise. The global term makes curves avoid falling into local minima, and the local term takes local feature information into consideration to provide more accurate evolving direction in the region with intensity inhomogeneity. By this means, we can finally obtain complete and correct contours.

4.2.2 Comparison of segmentation accuracy

In this section, F values are calculated to evaluate the segmentation results in a quantitative way. As shown in Fig.6, the binary segmentation results corresponding to above-mentioned 6 ACMs, proposed method and the ground truth are presented.

Table 2 Statistical results of F values.

IR image	GAC	CV	SLGS	LPF	LoG&RSF	LIC	Ours
1	0.2031	0.9599	0.9013	0.7690	0.7044	0.5395	0.9535
2	0.4729	0.9540	0.9682	0.7137	0.6903	0.8824	0.9793
3	0.2058	0.9175	0.9172	0.5164	0.6318	0.9632	0.9897
4	0.2976	0.9646	0.9614	0.8139	0.7807	0.9240	0.9669
5	0.1003	0.9443	0.9450	0.7312	0.7653	0.9682	0.9868
6	0	0.9807	0.9656	0.6171	0.6816	0.9771	0.9792
7	0.0641	0.9673	0.9711	0.0777	0.0924	0.9391	0.9732
8	0.0536	0.9355	0.9658	0.0670	0.0879	0.8938	0.9698
9	0.5889	0.9183	0.9254	0.8869	0.7736	0.8751	0.9277
10	0.1003	0.9538	0.9496	0.6147	0.6618	0.9682	0.9843
11	0.2695	0.9668	0.9722	0.6862	0.6819	0.9475	0.9836
12	0.2104	0.9536	0.9512	0.6895	0.7381	0.9706	0.9834
13	0.0356	0.9267	0.9395	0.6632	0.6817	0.7557	0.9509
14	0	0.9676	0.9630	0.7505	0.7218	0.6587	0.9792
15	0.2975	0.3414	0.9198	0.8771	0.8430	0.3236	0.9347
16	0.3111	0.8342	0.9149	0.6185	0.5549	0.5827	0.9450
Ave.	0.2007	0.9054	0.9457	0.6308	0.6307	0.8231	0.9680

The F values of 16 IR images segmented by 6 traditional ACMs and our method are listed in Table.2, and the top three largest F values are marked in red, green and blue, respectively. From Table.2, we find that the F values of GAC model are the worst among all the ACMs. That is because GAC model can detect the real object boundary only when the contour is initialized in specific locations. The contour is initialized in the image center in this experiment, which cannot contain the objects of interest completely, thus the results are poor. CV model and SLGS model can automatically detect all the boundaries in the image, regardless of the location of initial contour. As a result,

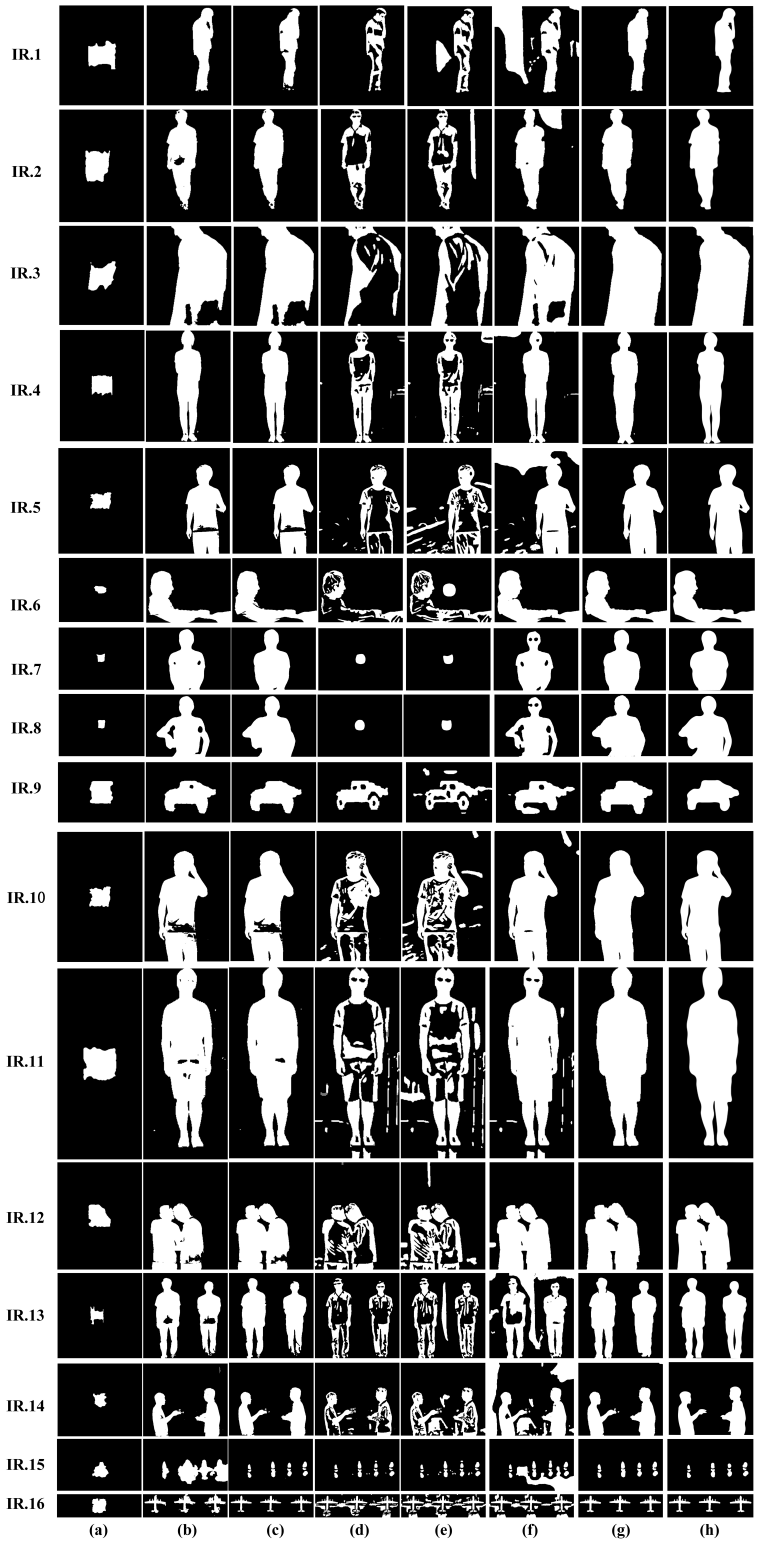

Fig. 6 Binary segmentation results of ACMs: (a) GAC; (b) CV; (c) SLGS; (d) LPF; (e) LoG & RSF; (f) LIC; (g) the proposed method; (h) ground truth.

their F values are higher than GAC model. However, when the IR images are with severe local intensity inhomogeneity, global gray average information cannot drive the evolving curve stopping correctly. Under the circumstances, over segmentation and boundary leakage occur and F values decrease remarkably. As for LPF model and LoG & RSF model, they only consider local intensity information, but ignore the global information. Therefore, they are prone to local minimum, leading to the result that the object is divided into many blocks mistakenly and the average F values of these two models are mediocre in our comparative experiments. LIC model which combines ACMs with bias eld estimation is another strategy to cope with intensity inhomogeneity, but it is only suitable for images with simple background. So, the F values of LIC model are sometimes unsatisfactory because the curves are unable to converge in complex background regions. Compared to the above-mentioned ACMs, our method is able to get acceptable F value of each test IR image and the average F value is also the largest, i.e., the proposed method can detect real object boundary more accurately and deal with inhomogeneous region more effectively.

4.2.3 Comparison of running time

In addition to F value, running time is also employed as a metric to evaluate our algorithm. Using the same experimental platform, the running time of different models is reported in Table.3 and the top three fastest ACMs have been marked in red, green and blue, respectively.

Table 3 Comparison of running time (in seconds).

IR image	GAC	CV	SLGS	LPF	LoG&RSF	LIC	Ours
1	18.1139	13.5297	3.3378	20.7844	20.4282	14.9276	6.0533
2	27.3372	12.3852	2.9496	7.3727	12.1505	9.1231	3.6548
3	27.1972	9.1124	2.9798	19.5277	24.8085	14.2686	3.0182
4	70.0298	10.1436	20.5524	21.2821	50.8191	13.5070	12.6598
5	88.6933	12.1157	9.8170	13.8495	22.7730	44.8938	13.8233
6	40.8549	33.9340	4.1179	34.8879	23.7596	12.2659	5.8662
7	87.3778	75.4667	13.6767	37.7720	33.9261	12.9943	18.2724
8	87.2557	105.3378	14.6998	75.2106	33.8854	17.1493	19.0991
9	28.7005	4.9718	2.6225	5.6645	12.0644	16.4423	8.8490
10	99.0442	28.0527	11.5100	44.3073	40.4406	27.6962	22.1138
11	38.8612	15.9982	4.2488	12.3188	30.9024	7.5761	8.6286
12	99.5036	18.9900	5.5146	15.7955	25.1829	9.6633	7.2771
13	174.6654	29.7931	7.3969	35.9777	51.1787	29.0758	9.7427
14	105.9294	19.8835	6.9861	59.6416	61.7432	25.5123	15.4654
15	47.5315	18.7070	5.1385	14.7697	18.8393	43.9738	6.8167
16	27.2223	5.5518	2.8613	6.8161	11.1171	3.3074	6.6630
Ave.	66.7699	25.8733	7.4006	26.6236	29.6262	18.8985	10.5002

As shown in Table.3, it is notable that GAC model and CV model are time-consuming due to their relatively poor convergence. The average running time of GAC model and CV model is approximately 6 times and 2.5 times longer

than that of our algorithm. LPF model is a fast image segmentation model because it computes the pre-fitting functions before the evolution of curve and the pre-tting functions do not need to update in each iteration. However, LPF model needs to minimize the local energy function so that plenty of time is needed during this procedure. Although LoG & RSF model imposes optimized LoG operator to detect the edge more effectively, but similar to LPF model, it still costs a lot of time to converge. As a result, the execution efficiencies of LPF and LoG & RSF model are moderate in the whole comparison. LIC model achieves satisfactory running time in some test images with simple background but performs poorly in others. Therefore, its calculation time is directly decided by the characteristics of image. SLGS model gets the fastest execution speed because it only needs to calculate the global intensity information to guide curve evolution, so its running efficiency is the highest. As for our method, the average running time is only longer than SLGS model (approximately 3 seconds longer), because we introduce the local feature to reform the SPF function. We plan to transplant our algorithm to higher-speed computing platform and achieve real-time running in the future work. Considering the accuracy of segmentation results, we can draw a conclusion that our method can obtain desirable results and acceptable execution time in IR image segmentation.

5 Conclusion

In this paper, to segment IR images with intensity inhomogeneity effectively, we design a special SPF function which contains not only global information but also local feature information. Firstly, the global term computed by global gray average information guides the evolving curve to pass through the background region quickly and prevents the evolving curve falling into local minimum. The local term calculated by local entropy, local standard deviation and gradient information provides more local information to determine the evolution direction more precisely in real boundary region. Then, the global term and local term are combined by an adaptive weight coefficient based on local range information so as to construct the complete SPF function. Next, LSF is rewritten by the new SPF function and meanwhile a Gaussian filter is utilized to re-initialize LSF. By finite iterations, we finally obtain the contour of object according to the zero LSF. Both qualitative and quantitative experiments are implemented to compare this proposed algorithm with other ACMs, proving that our method outperforms the comparing ones in terms of precision rate and overlapping rate. To further decrease the running time, we plan to execute our proposed algorithm in high-speed computing platform in the future.

Acknowledgement

This research was supported by National Natural Science Foundation of China (No. 62001234), Natural Science Foundation of Jiangsu Province (No. BK20200487), China Postdoctoral Science Foundation (No. 2020M681597) and Postdoctoral Science Foundation of Jiangsu Province (No. 2020Z051).

Conflict of interest

The authors declare no conflict of interest.

References

1. Fengler, J., Westwick, P., Bailey, A.E., Cottle, P.: Imaging system for combined full-color reflectance and near-infrared imaging (2015). US Patent 9,173,554
2. Izadi, H., Sadri, J., Hormozzade, F., Fattahpour, V.: Altered mineral segmentation in thin sections using an incremental-dynamic clustering algorithm. Engineering Applications of Artificial Intelligence **90**, 103466 (2020)
3. Xu, J., Wang, H., Cui, C., Liu, P., Zhao, Y., Li, B.: Oil spill segmentation in ship-borne radar images with an improved active contour model. Remote Sensing **11**(14), 1698 (2019)
4. Yang, Y., Lin, L.: Automatic pedestrians segmentation based on machine learning in surveillance video. In: 2019 IEEE International Conference on Computational Electromagnetics (ICCEM), pp. 1–3. IEEE (2019)
5. Xu, D., Zhang, G., You, Z.: Adaptive segmentation and feature acquisition of test sequence for momentum wheel. IEEE Access **7**, 153278–153286 (2019)
6. Naz, S., Majeed, H., Irshad, H.: Image segmentation using fuzzy clustering: A survey. In: 2010 6th international conference on emerging technologies (ICET), pp. 181–186. IEEE (2010)
7. Hagagg, S., Khalifa, F., Abdeltawab, H., Elnakib, A., Abdelazim, M., Ghazal, M., Sandhu, H., El-Baz, A.: A cnn-based framework for automatic vitreous segemntation from oct images. In: 2019 IEEE International Conference on Imaging Systems and Techniques (IST), pp. 1–5. IEEE (2019)
8. Meiju, L., Rui, Z., Xifeng, G., Junrui, Z.: Application of improved otsu threshold segmentation algorithm in mobile phone screen defect detection. In: 2020 Chinese Control And Decision Conference (CCDC), pp. 4919–4924. IEEE (2020)
9. Kass, M., Witkin, A., Terzopoulos, D.: Snakes: Active contour models. International journal of computer vision **1**(4), 321–331 (1988)
10. Wan, M., Gu, G., Sun, J., Qian, W., Ren, K., Chen, Q., Maldague, X.: A level set method for infrared image segmentation using global and local information. Remote Sensing **10**(7), 1039 (2018)
11. Lu, C.S., Chung, P.C., Chen, C.F.: Unsupervised texture segmentation via wavelet transform. Pattern recognition **30**(5), 729–742 (1997)
12. Lee, L.K., Liew, S.C., Thong, W.J.: A review of image segmentation methodologies in medical image. In: Advanced computer and communication engineering technology, pp. 1069–1080. Springer (2015)
13. Wang, C., Wang, Y., Kaba, D., Wang, Z., Liu, X., Li, Y.: Automated layer segmentation of 3d macular images using hybrid methods. In: International Conference on Image and Graphics, pp. 614–628. Springer (2015)
14. Zhang, T., Han, J., Zhang, Y., Bai, L.: An adaptive multi-feature segmentation model for infrared image. Optical Review **23**(2), 220–230 (2016)
15. Caselles, V., Kimmel, R., Sapiro, G.: Geodesic active contours. In: Proceedings of IEEE international conference on computer vision, pp. 694–699. IEEE (1995)

16. Paragios, N., Mellina-Gottardo, O., Ramesh, V.: Gradient vector flow fast geodesic active contours. In: Proceedings Eighth IEEE International Conference on Computer Vision. ICCV 2001, vol. 1, pp. 67–73. IEEE (2001)
17. Wang, Q.: The improvement of gac model for image segmentation. In: 2013 IEEE 4th International Conference on Software Engineering and Service Science, pp. 1021–1024. IEEE (2013)
18. Ronfard, R.: Region-based strategies for active contour models. International journal of computer vision **13**(2), 229–251 (1994)
19. Chan, T.F., Vese, L.A.: Active contours without edges. IEEE Transactions on image processing **10**(2), 266–277 (2001)
20. Li, C., Kao, C.Y., Gore, J.C., Ding, Z.: Minimization of region-scalable fitting energy for image segmentation. IEEE transactions on image processing **17**(10), 1940–1949 (2008)
21. Ding, K., Xiao, L., Weng, G.: Active contours driven by local pre-fitting energy for fast image segmentation. Pattern Recognition Letters **104**, 29–36 (2018)
22. Liu, S., Peng, Y.: A local region-based chan–vese model for image segmentation. Pattern Recognition **45**(7), 2769–2779 (2012)
23. Wang, L., Zhang, L., Yang, X., Yi, P., Chen, H.: Level set based segmentation using local fitted images and inhomogeneity entropy. Signal Processing **167**, 107297 (2020)
24. Ding, K., Xiao, L., Weng, G.: Active contours driven by region-scalable fitting and optimized laplacian of gaussian energy for image segmentation. Signal Processing **134**, 224–233 (2017)
25. Li, C., Huang, R., Ding, Z., Gatenby, J.C., Metaxas, D.N., Gore, J.C.: A level set method for image segmentation in the presence of intensity inhomogeneities with application to mri. IEEE transactions on image processing **20**(7), 2007–2016 (2011)
26. Zhang, K., Zhang, L., Lam, K.M., Zhang, D.: A level set approach to image segmentation with intensity inhomogeneity. IEEE transactions on cybernetics **46**(2), 546–557 (2015)
27. Huang, G., Ji, H., Zhang, W.: A fast level set method for inhomogeneous image segmentation with adaptive scale parameter. Magnetic resonance imaging **52**, 33–45 (2018)
28. Min, H., Jia, W., Zhao, Y.: A region-bias fitting model based level set for segmenting images with intensity inhomogeneity. In: Proceedings of the 2nd International Symposium on Image Computing and Digital Medicine, pp. 83–87 (2018)
29. Shan, X., Gong, X., Nandi, A.K.: Active contour model based on local intensity fitting energy for image segmentation and bias estimation. IEEE Access **6**, 49817–49827 (2018)
30. Zhang, K., Zhang, L., Song, H., Zhou, W.: Active contours with selective local or global segmentation: a new formulation and level set method. Image and Vision computing **28**(4), 668–676 (2010)
31. Mukherjee, S., Acton, S.T.: Region based segmentation in presence of intensity inhomogeneity using legendre polynomials. IEEE Signal Processing Letters **22**(3), 298–302 (2014)
32. DONG, E.z., FENG, Q., YU, X., TONG, J.g., GU, H.q.: Improved contour extraction algorithm of infrared images based on active contour models. Laser & Infrared (3), 25 (2017)

Figures

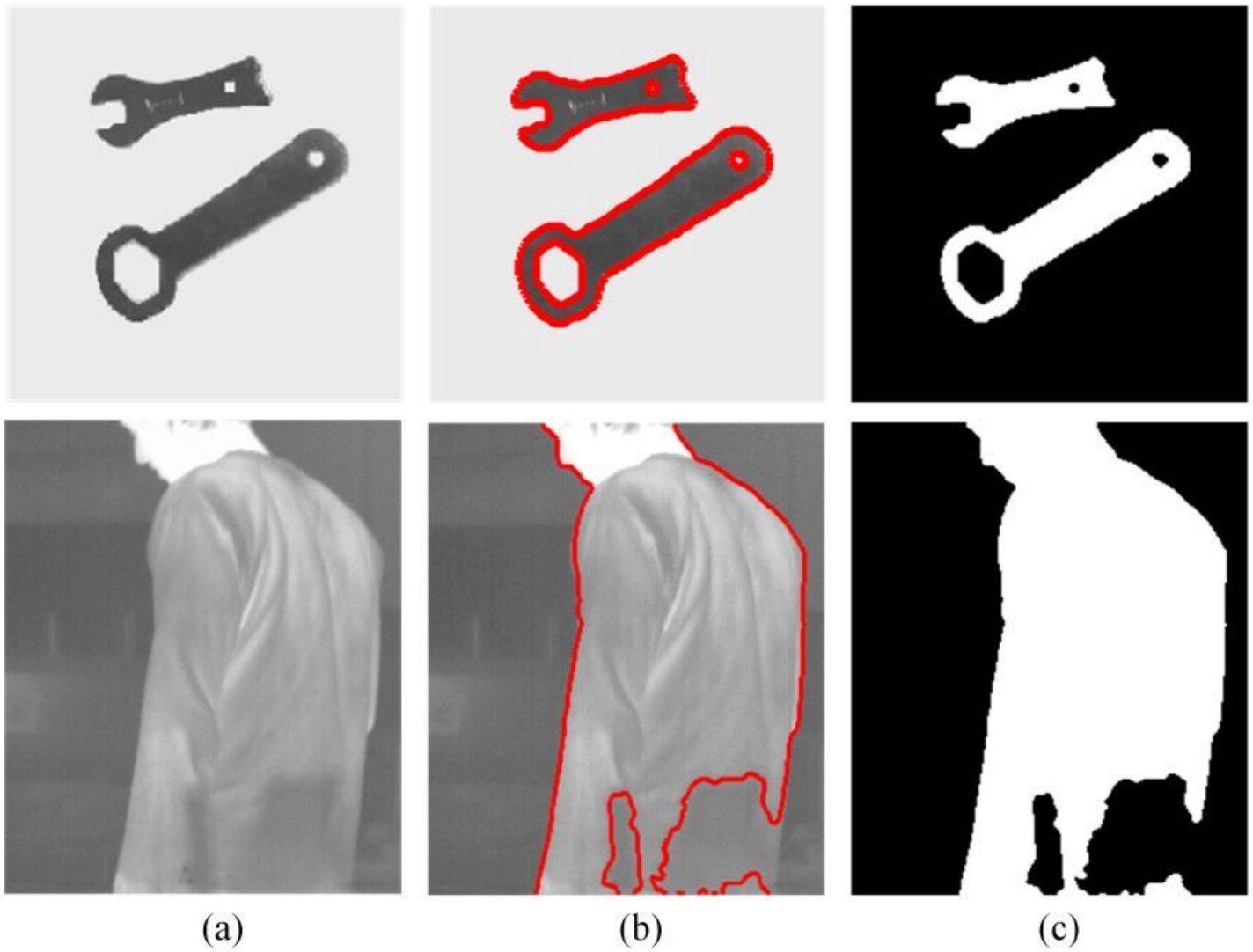

Figure 1

Segmentation results of SLGS model: (a) original image; (b) segmentation result; (c) binary segmentation result.

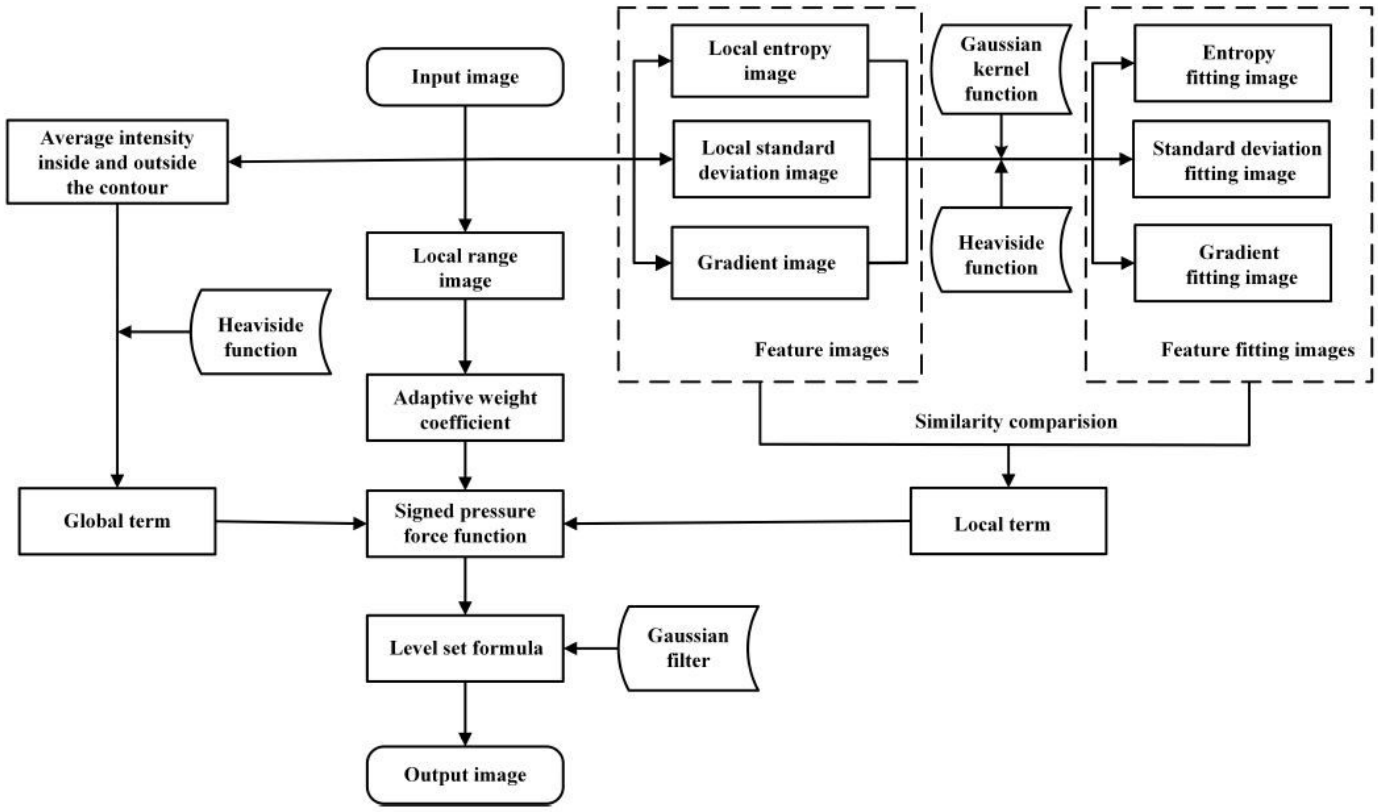

Figure 2

Structure diagram of the proposed method.

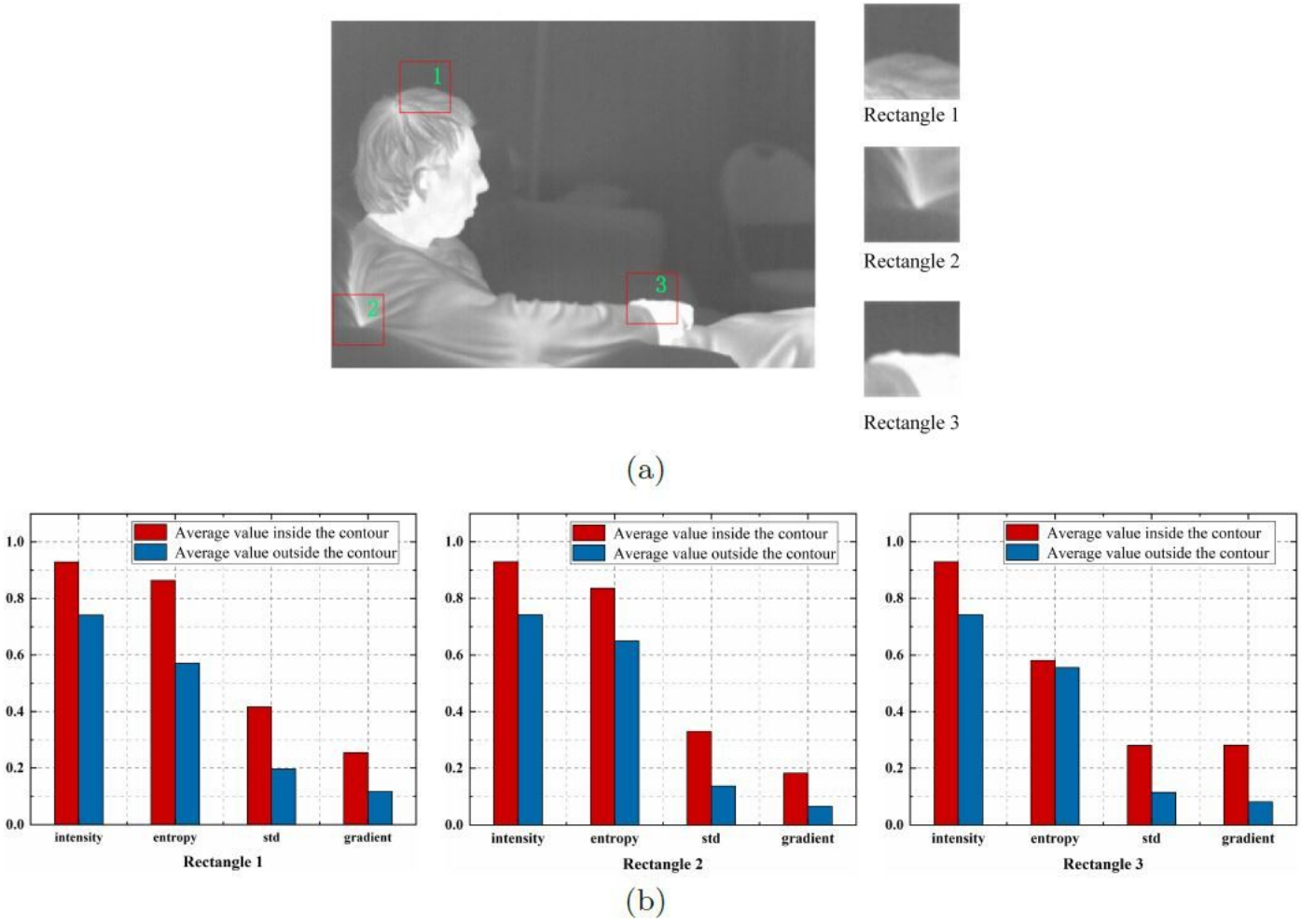

Figure 3

Comparative analysis of local features: (a) local area of original image; (b) average values of different features in rectangle 1, rectangle 2 and rectangle 3 respectively, red charts represent the average of object, blue charts represent the average of background.

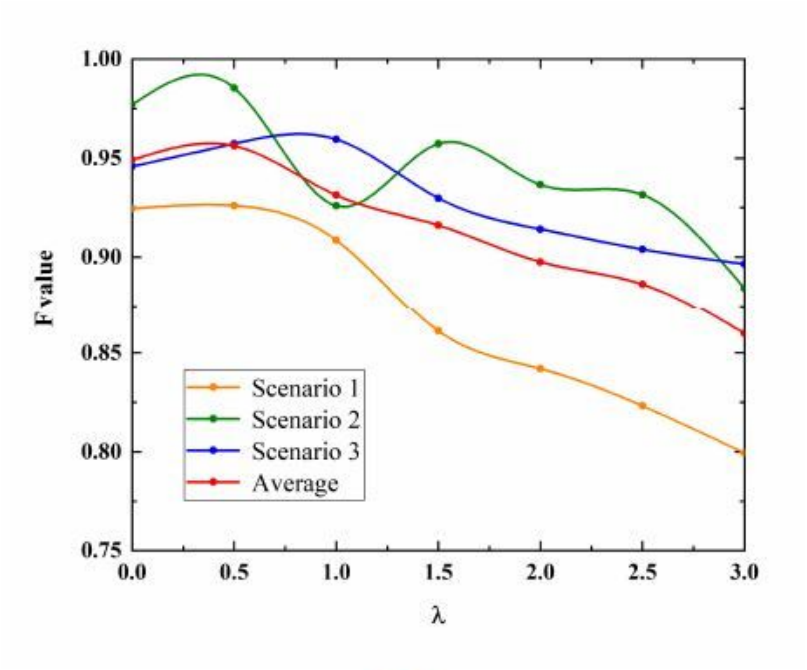

(a)

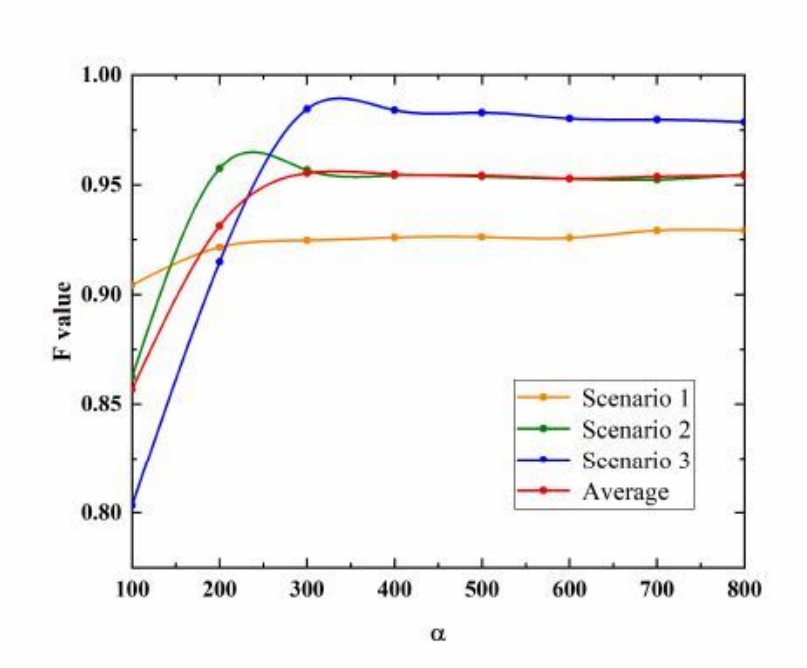

(b)

Figure 4

Sensitivity analysis: (a)F - λ curves; (b) F - α curves.

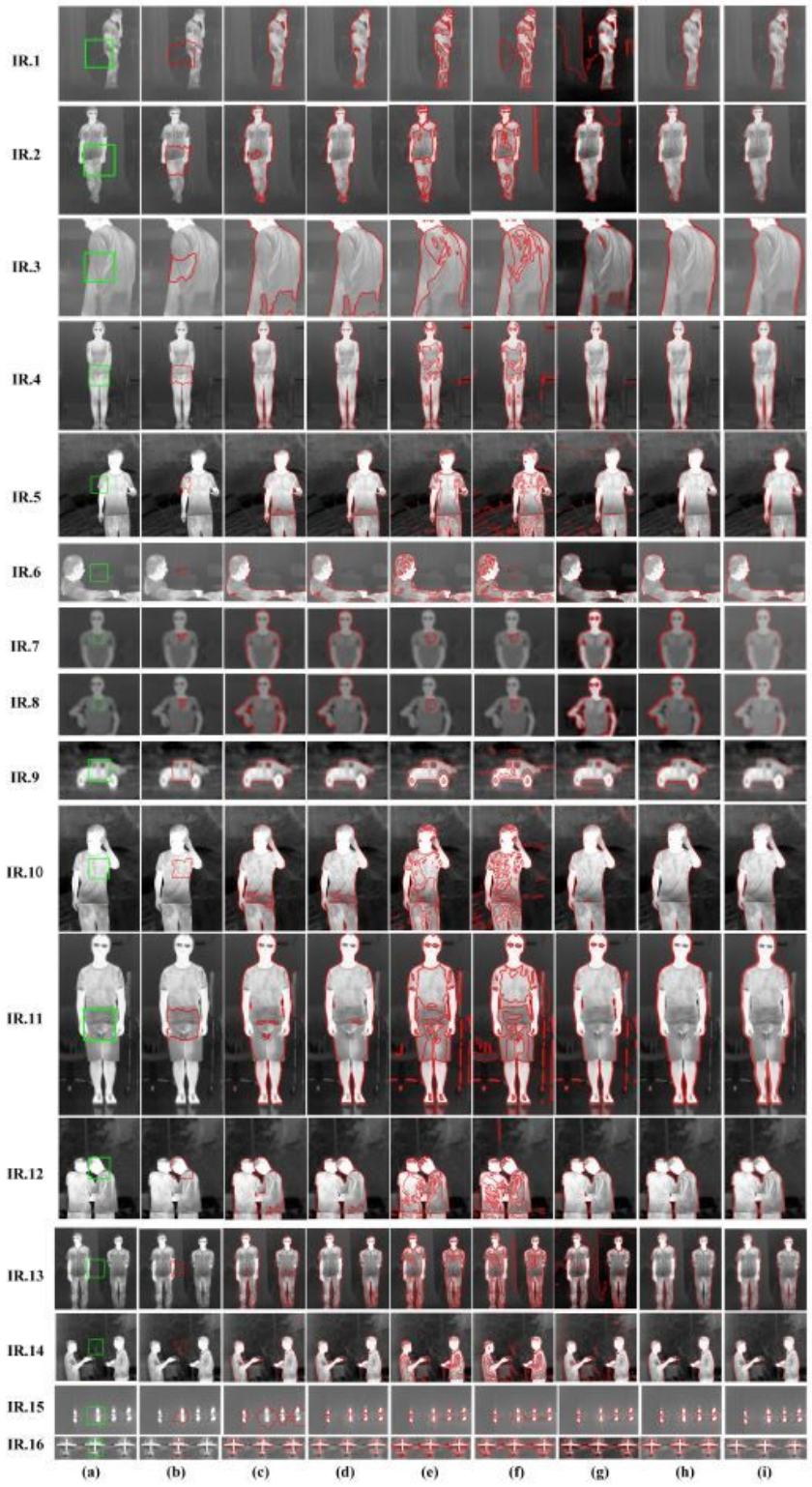

Figure 5

Segmentation results of ACMs: (a) initial contour; (b) GAC; (c) CV; (d) SLGS; (e) LPF; (f) LoG & RSF; (g) LIC; (h) the proposed method; (i) ground truth.

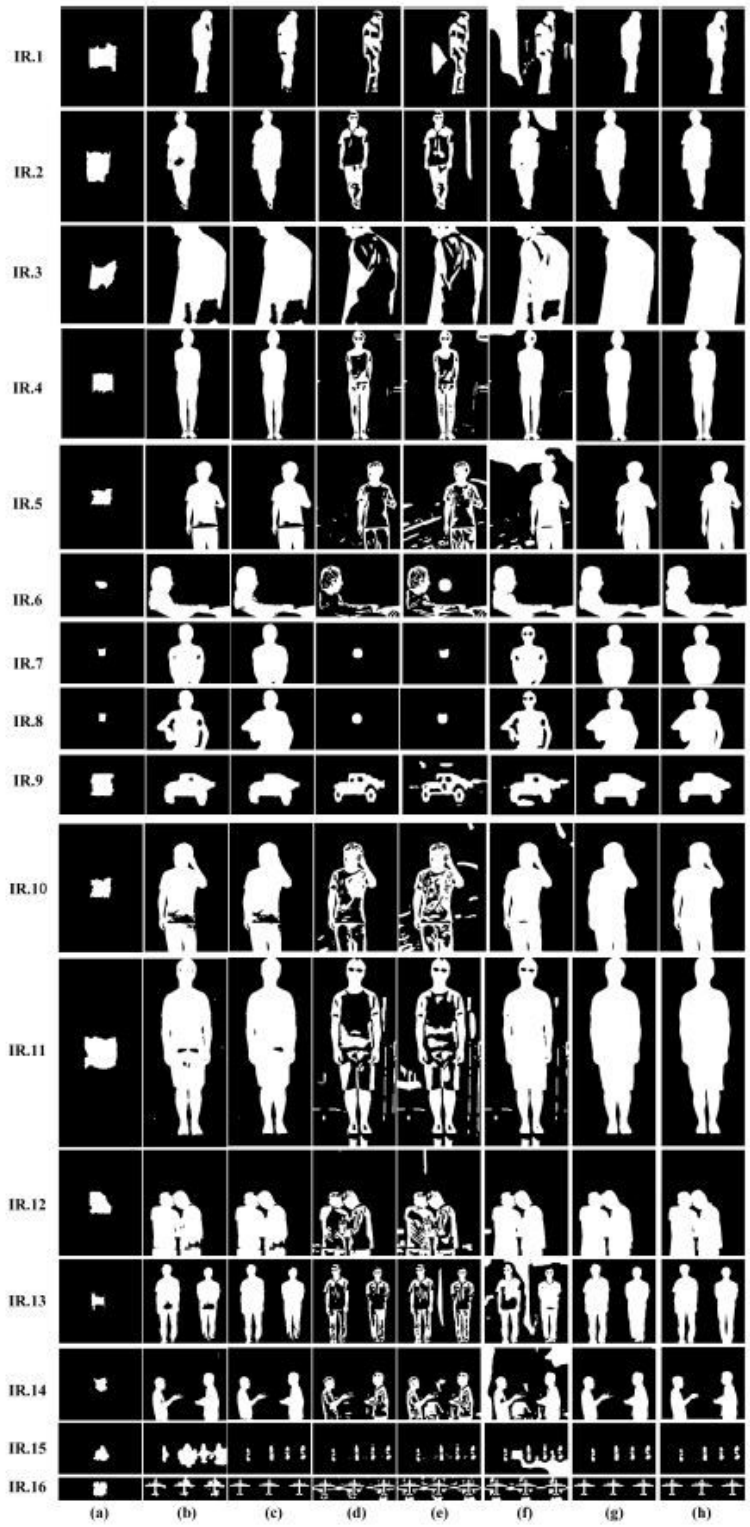

Figure 6

Binary segmentation results of ACMs: (a) GAC; (b) CV; (c) SLGS; (d) LPF; (e) LoG & RSF; (f) LIC; (g) the proposed method; (h) ground truth.